Ocean Acoustic Tomography as a Data Assimilation Problem

Pierre Elisseeff, Henrik Schmidt, and Wen Xu, *Member, IEEE*

***Abstract*—The ocean acoustic tomographic (OAT) approach to sound speed field estimation is generalized to include a variety of sources of information of interest such as an oceanographic model of the sound speed field, direct local sound speed measurements, and a full field acoustic propagation model as well as measurements. The inverse problem is presented as a four-dimensional field estimation problem using a variational approach commonly used in oceanographic data assimilation. The current OAT approach is shown to be a special case of the general framework. The matched-field tomography (MFT) approach is also discussed within this context. A simple implementation of this novel approach is then investigated in the absence of a suitable oceanographic model, and acoustic propagation is accounted for using a standard parabolic equation model. The inverse equations derived are validated numerically through a simple inversion example, and some issues on environmental mismatch and computations are discussed. The developments then provide a basic framework for ongoing data-model melding in acoustically focused oceanographic sampling (AFOS) network.**

***Index Terms*—Acoustic data assimilation, acoustically focused oceanographic sampling, ocean acoustic tomography.**

I. Introduction

RECENT advances in sensor technology and computing power have made relatively large data streams of heterogeneous nature available to oceanographers, sampling the oceanic environment both locally and remotely. Concurrent advances in acoustical modeling have made it possible to accurately predict acoustic propagation characteristics provided adequate environmental information is available. By combining both data and modeling assets in an operational setting, acoustically focused oceanographic sampling (AFOS) will enable rapid assessment of oceanic fields while drawing on the strength of individual data types, i.e., the large coverage of integral acoustic measurements and the high resolution of local direct measurements [1]. The Haro Strait experiment was implemented in June–July 1996 near Victoria, British Columbia, Canada, in order to test a number of engineering and scientific concepts related to coastal oceanic field estimation [2]. The experiment showed that synoptic field estimates can be produced in real time for oceanographically challenging regions, provided that inversion algorithms are kept simple and linear while sustaining environmental and system uncertainties. It also showed that multiple heterogeneous data streams are necessary in order to overcome the inherent limitations of each data type.

While ocean acoustic tomography (OAT) was used for the acoustic measurement model in Haro Strait, it became clear soon after the experiment that the current OAT formulation [3] has many limitations with regard to efficient field estimation. Drawing on the oceanographic data assimilation literature, the efficient combination of data and models into a field estimate requires the following: a measurement model, capturing the data measurement process; a dynamical model, capturing the deterministic physics of the observed physical process, and *a priori* statistics for both the data and the model error fields [4]. Most OAT applications solely use the travel-time measurement, which is often doubly approximate as it is perturbative and based on resolvable ray or modal arrivals. Some modified versions (e.g., a recent one based on peak arrivals [5]) are developed to avoid the identification of actual arrivals as ray or modal ones, but the full field propagation including unresolved ray/modal arrivals has not been included in general, which is especially important in coastal, shallow water. Furthermore, the OAT approach does provide *a priori* statistics for the data and the sound speed field; however, capturing the deterministic spatial and temporal physical structure of the sound speed field is hardly exercised.

To palliate these shortcomings and assimilate acoustic data into models, a novel framework is developed. This framework lays out explicitly a set of four defining equations driven by additive noise terms as outlined in the next section. The resulting sound speed and pressure field estimates agree with both the data and the models within their respective error bounds. Data assimilation has been well developed in ocean observing and prediction systems (OOPS) [4], but its application to underwater acoustics is just started. The generalized approach represents a first step toward the assimilation of acoustic data into ocean models, and can therefore be referred to as *acoustic data assimilation*.

The example shown in this paper focuses on spatial estimation although time is implicitly taken into account in the formulation. The inversion framework is outlined in the next section. The special cases of OAT and matched-field tomography (MFT) are then investigated. A practical implementation based on the standard parabolic equation model is presented in the following section. Finally, numerical results are shown and discussed.

Manuscript received January 7, 2002. This work was supported by the Office of Naval Research under Grant N00014-97-1-1018.

P. Elisseeff was with the Department of Ocean Engineering, Massachusetts Institute of Technology, Cambridge, MA 02139 USA. He is now with Dean & Company, Vienna, VA 22182 USA.

H. Schmidt and W. Xu are with the Department of Ocean Engineering, Massachusetts Institute of Technology, Cambridge, MA 02139 USA (e-mail: wenxu@mit.edu).

Publisher Item Identifier S 0364-9059(02)03369-1.

II. The Inverse Problem

A. General Inverse Formulation

Information regarding the ocean sound speed field can be drawn from a number of sources when trying to solve the sound speed field inversion problem. Acoustic pressure measurements $\tilde{\mathbf{p}}$ of the acoustic pressure field $\mathbf{p}$ are gathered by acoustic arrays surrounding the region of interest. Direct (local) measurements $\tilde{\mathbf{c}}$ of the sound speed field $\mathbf{c}$ might be available, e.g., through CTD data sets. An acoustic wave propagation model $\boldsymbol{\mathcal{B}}$, chosen for its relevance to a particular operational scenario, provides a link between the acoustic measurements and the sound speed field. In addition, further information regarding the spatial and temporal structure of the sound speed field might be contained in what can be loosely called an oceanographic model $\boldsymbol{\mathcal{A}}$. This model may be a simple stochastic constraint or a complex ocean circulation model. These four sources of information are encapsulated in the following set of equations:

$$\tilde{\mathbf{c}} = \mathbf{M}\mathbf{c} + \mathbf{c}_n, \qquad \mathbf{c}_n \sim N(\mathbf{0}, \mathbf{R}_c) \tag{1}$$

$$\mathcal{A}(\mathbf{c}) = \mathbf{v}, \qquad \mathbf{v} \sim N(\mathbf{0}, \mathbf{Q}_a) \tag{2}$$

$$\mathcal{B}(\mathbf{p}, \mathbf{c}) = \mathbf{w}, \qquad \mathbf{w} \sim N(\mathbf{0}, \mathbf{Q}_b) \tag{3}$$

$$\tilde{\mathbf{p}} = \mathbf{L}\mathbf{p} + \mathbf{p}_n, \qquad \mathbf{p}_n \sim N(\mathbf{0}, \mathbf{R}_p) \tag{4}$$

where $\mathbf{M}$ and $\mathbf{L}$ denote mapping from the true (sound speed or pressure) field to individual measurement points (e.g., the coordinate mapping) and $\mathbf{R}_c$, $\mathbf{Q}_a$, $\mathbf{Q}_b$, and $\mathbf{R}_p$ denote the covariance matrices of individual noise models. The first equation corresponds to the *local sound speed measurement model*. The Gaussian noise vector $\mathbf{c}_n$ accounts for local sampling errors. The second equation corresponds to the *oceanographic dynamical model*, thus called by analogy with the oceanographic data assimilation problem. It is driven by the Gaussian noise vector $\mathbf{v}$ accounting for unmodeled features of the sound speed field. The third equation corresponds to the *acoustic dynamical model*. It relates the true pressure field to the true sound speed field. It is driven by the Gaussian noise vector $\mathbf{w}$ accounting for model uncertainties such as surface roughness, bottom composition, bathymetric uncertainties, and sensor locations. The fourth equation corresponds to the *acoustic pressure measurement model*. The additive noise component is here again modeled as a Gaussian random vector with known covariance matrix.

The inverse problem now amounts to the estimation of the two state vectors $\mathbf{p}$ and $\mathbf{c}$. Note that the sound speed field $\mathbf{c}$ is understood in general terms; the equations described in this section remain the same regardless of whether $\mathbf{c}$ represents the actual sound speed field, a set of EOF coefficients, or any other adequate mapping. Following the traditional variational approach, an optimal estimate of the sound speed field can be computed by minimizing the misfit between the available data sets and the available models, i.e., by jointly minimizing the mean square errors of (1)–(4)

$$\hat{\mathbf{c}} = \underset{\mathbf{p},\,\mathbf{c}}{\arg\min}\,\{J(\mathbf{p}, \mathbf{c})\} \tag{5}$$

where the objective function J is given by

$$J(\mathbf{p}, \mathbf{c}) = \mathbf{c}_n^\dagger \mathbf{R}_c^{-1} \mathbf{c}_n + \mathbf{v}^\dagger \mathbf{Q}_a^{-1} \mathbf{v} + \mathbf{w}^\dagger \mathbf{Q}_b^{-1} \mathbf{w} + \mathbf{p}_n^\dagger \mathbf{R}_p^{-1} \mathbf{p}_n. \tag{6}$$

Formally minimizing the objective function given above yields

$$\mathbf{L}^\dagger \mathbf{R}_p^{-1} \mathbf{L}\mathbf{p} + \frac{\partial \boldsymbol{\mathcal{B}}^\dagger}{\partial \mathbf{p}}\, \mathbf{Q}_b^{-1} \boldsymbol{\mathcal{B}} = \mathbf{L}^\dagger \mathbf{R}_p^{-1} \tilde{\mathbf{p}} \tag{7}$$

$$\frac{\partial \boldsymbol{\mathcal{B}}^\dagger}{\partial \mathbf{c}}\, \mathbf{Q}_b^{-1} \boldsymbol{\mathcal{B}} + \frac{\partial \boldsymbol{\mathcal{A}}^\dagger}{\partial \mathbf{c}}\, \mathbf{Q}_a^{-1} \boldsymbol{\mathcal{A}} + \mathbf{M}^\dagger \mathbf{R}_c^{-1} \mathbf{M}\mathbf{c} = \mathbf{M}^\dagger \mathbf{R}_c^{-1} \tilde{\mathbf{c}}. \tag{8}$$

The system of equations (7) and (8) is coupled through two separate entities. The first is as expected the acoustic model $\boldsymbol{\mathcal{B}}$: it formally relates the acoustic pressure field to the sound speed field. The second entity is the covariance matrix associated with the acoustic dynamical model, i.e., the model error covariance matrix $\mathbf{Q}_b$. If the model error statistics are not quantified, the eigenvalues of $\mathbf{Q}_b$ become infinite, thus expressing the fact that no information is available regarding possible model errors. The inverse of $\mathbf{Q}_b$ then tends toward zero and equations (7) and (8) become uncoupled. Equation (7) then reduces to the problem of estimating the acoustic pressure field given the acoustic data only. Equation (8) reduces to the oceanographic data assimilation problem in the absence of acoustic data. In order to preserve the natural coupling exhibited by (7) and (8), and therefore optimally estimate the sound speed field using both the available data sets and the available models, error fields must be carefully quantified through the different covariance matrices in general and $\mathbf{Q}_b$ in particular. Jointly solving (7) and (8) will yield an optimal sound speed estimate $\hat{\mathbf{c}}$ which will agree with all data sets and models available *within their respective error bounds*. In particular this estimate will include the full physics of wave propagation and possibly ocean circulation as specified by (2) and (3). As a byproduct, the acoustic field will also be estimated.

An alternate version of the system of equations (7) and (8) can be derived when the acoustic dynamical model $\boldsymbol{\mathcal{B}}(\mathbf{p}, \mathbf{c})$ is written as $\mathbf{p} - \boldsymbol{\Phi}(\mathbf{c})$ and the oceanographic dynamical model $\boldsymbol{\mathcal{A}}(\mathbf{c})$ is written as $\mathbf{c} - \boldsymbol{\Psi}$

$$\left(\mathbf{L}^\dagger \mathbf{R}_p^{-1} \mathbf{L} + \mathbf{Q}_b^{-1}\right) \mathbf{p} = \mathbf{L}^\dagger \mathbf{R}_p^{-1} \tilde{\mathbf{p}} + \mathbf{Q}_b^{-1} \boldsymbol{\Phi} \tag{9}$$

$$\frac{\partial \boldsymbol{\Phi}}{\partial \mathbf{c}}\, \mathbf{Q}_b^{-1} \boldsymbol{\Phi} + \left(\mathbf{M}^\dagger \mathbf{R}_c^{-1} \mathbf{M} + \mathbf{Q}_a^{-1}\right) \mathbf{c} = \mathbf{M}^\dagger \mathbf{R}_c^{-1} \tilde{\mathbf{c}} + \mathbf{Q}_a^{-1} \boldsymbol{\Psi} + \frac{\partial \boldsymbol{\Phi}}{\partial \mathbf{c}}\, \mathbf{Q}_b^{-1} \mathbf{p} \tag{10}$$

where $\boldsymbol{\Phi}$ represents an acoustic propagation model which takes $\mathbf{c}$ as input and returns $\mathbf{p}$ as output and $\boldsymbol{\Psi}$ represents an oceanographic model whose input is independent of both $\mathbf{p}$ and $\mathbf{c}$ and returns $\mathbf{c}$ as output. This alternate set of equations may be more suitable to some numerical implementations, in particular when derivatives of the acoustic model are available, e.g., through automated differentiation tools such as TAMC [6].

B. Simplified Inverse Formulation

In many cases, an oceanographic dynamical model is not available, either because the region of interest is poorly understood, or because such a model is computationally too demanding. Furthermore, direct sound speed measurements might not be included in the inversion, either because they do not exist, or because they are used independently for validation purposes. In this case, which

is of practical relevance to many ocean acoustic applications, the original set of equations (1)–(4) becomes

$$\mathbf{c} - \mathbf{c}_0 = \mathbf{c}_n, \qquad \mathbf{c}_n \sim N(\mathbf{0}, \mathbf{S}) \tag{11}$$

$$\mathcal{B}(\mathbf{p}, \mathbf{c}) = \mathbf{w}, \qquad \mathbf{w} \sim N(\mathbf{0}, \mathbf{Q}_b) \tag{12}$$

$$\tilde{\mathbf{p}} = \mathbf{L}\mathbf{p} + \mathbf{p}_n, \qquad \mathbf{p}_n \sim N(\mathbf{0}, \mathbf{R}_p) \tag{13}$$

where $\mathbf{S}$ is the covariance matrix of the random sound speed perturbation. Equation (11) simply expresses the fact that the sound speed field is now modeled as a random vector of known statistics. This is the weakest practical constraint which can be imposed upon $\mathbf{c}$. The objective function becomes

$$J(\mathbf{p}, \mathbf{c}) = \mathbf{c}_n^\dagger \mathbf{S}^{-1} \mathbf{c}_n + \mathbf{w}^\dagger \mathbf{Q}_b^{-1} \mathbf{w} + \mathbf{p}_n^\dagger \mathbf{R}_p^{-1} \mathbf{p}_n. \tag{14}$$

Minimizing the objective function leads to the following set of equations:

$$\mathbf{L}^\dagger \mathbf{R}_p^{-1} \mathbf{L}\mathbf{p} + \frac{\partial \boldsymbol{\mathcal{B}}^\dagger}{\partial \mathbf{p}} \mathbf{Q}_b^{-1} \boldsymbol{\mathcal{B}} = \mathbf{L}^\dagger \mathbf{R}_p^{-1} \tilde{\mathbf{p}} \tag{15}$$

$$\frac{\partial \boldsymbol{\mathcal{B}}^\dagger}{\partial \mathbf{c}} \mathbf{Q}_b^{-1} \boldsymbol{\mathcal{B}} + \mathbf{S}^{-1}(\mathbf{c} - \mathbf{c}_0) = \mathbf{0} \tag{16}$$

or alternatively

$$\left(\mathbf{L}^\dagger \mathbf{R}_p^{-1} \mathbf{L} + \mathbf{Q}_b^{-1}\right) \mathbf{p} = \mathbf{L}^\dagger \mathbf{R}_p^{-1} \tilde{\mathbf{p}} + \mathbf{Q}_b^{-1} \boldsymbol{\Phi} \tag{17}$$

$$\frac{\partial \boldsymbol{\Phi}}{\partial \mathbf{c}} \mathbf{Q}_b^{-1} \boldsymbol{\Phi} + \mathbf{S}^{-1}(\mathbf{c} - \mathbf{c}_0) = \frac{\partial \boldsymbol{\Phi}}{\partial \mathbf{c}} \mathbf{Q}_b^{-1} \mathbf{p}. \tag{18}$$

This system of equations can be solved by different methods. A simple method is outlined in Section III. A more general method would iterate over (15) and (16): assuming an initial sound speed guess, the acoustic pressure field can be estimated through (15). Then this estimate can be used in (16) in order to estimate the sound speed field. The algorithm converges as the associated data/model error bounds become narrower. The rate of convergence of this method may be improved by adapting the covariance matrix $\mathbf{Q}_b$ at each step in a way that reflects the relative information contents of the data set and the acoustic model. For instance, the acoustic model is expected to be fairly inaccurate at first. As the system is iterated the initial sound speed guess is refined and the acoustic model uncertainty may be expected to decrease accordingly. However, this procedure requires a formal error model which is beyond the scope of this paper and is still the object of active research.

C. Ocean Acoustic Tomography

The ocean acoustic tomographic problem is traditionally formulated in terms very similar to (11)–(13) although the acoustic dynamical model is in fact implicit and hidden in the acoustic measurement model [3]. It can be formally written as

$$\mathbf{c} = \mathbf{c}_n, \qquad \mathbf{c}_n \sim N(\mathbf{0}, \mathbf{S}) \tag{19}$$

$$\tilde{\boldsymbol{\tau}} = \mathbf{L}\mathbf{c} + \boldsymbol{\tau}_n, \qquad \boldsymbol{\tau}_n \sim N(\mathbf{0}, \mathbf{R}_\tau) \tag{20}$$

where the only state variable is $\mathbf{c}$ and the data $\boldsymbol{\tau}$ usually consists of arrival time perturbations. The objective function now reduces to two terms

$$J(\mathbf{c}) = \mathbf{c}_n^\dagger \mathbf{S}^{-1} \mathbf{c}_n + \boldsymbol{\tau}_n^\dagger \mathbf{R}_\tau^{-1} \boldsymbol{\tau}_n. \tag{21}$$

The optimal sound speed estimate is found once again by minimizing J

$$\hat{\mathbf{c}} = \left(\mathbf{L}^\dagger \mathbf{R}_\tau^{-1} \mathbf{L} + \mathbf{S}^{-1}\right)^{-1} \mathbf{L}^\dagger \mathbf{R}_\tau^{-1} \tilde{\boldsymbol{\tau}}. \tag{22}$$

This expression has been widely used in OAT inversions and can also be derived using a Bayesian maximum-likelihood approach [3]. A number of important limitations can be found in this OAT approach. The measurement model (20) aggregates a perturbative measurement model with an implicit ray(or modal)-theoretic dynamical model and is as such doubly approximate. The data used in the inversion excludes significant portions of the actual acoustic data acquired. By contrast, (1)–(4) or the simpler version (11)–(13) feature an exact acoustic measurement model where the matrix $\mathbf{L}$ simply contains the locations of the acoustic sensors on the computational grid. The data $\tilde{\mathbf{p}}$ include the full wave acoustic data acquired by the acoustic sensors. Furthermore, the acoustic dynamical model is cast in explicit form and is not limited to ray/modal models. As such, the inverse formulation outlined in Sections II-A and B can be viewed as a generalization of the OAT framework.

D. Matched-Field Tomography

The simplified inverse formulation outlined above can also be used to attempt to describe the MFT approach [7], [8]. The key difference is that the acoustic dynamical model is now assumed to be exact, i.e., the covariance matrix $\mathbf{Q}_b$ vanishes. Following the traditional MFT assumptions, the sound speed vector $\mathbf{c}$ is nonrandom but unknown, which can be expressed by the fact that the inverse covariance matrix $\mathbf{S}^{-1}$ vanishes. Using the alternate representation of $\mathcal{B}$ used in (9) and (10), which is also commonly used in MFT, the system of equations (11)–(13) then reduces to

$$\tilde{\mathbf{p}} = \mathbf{L}\boldsymbol{\Phi}(\mathbf{c}) + \mathbf{p}_n. \tag{23}$$

The objective function J has only one term left

$$J(\mathbf{c}) = \mathbf{p}_n^\dagger \mathbf{R}_p^{-1} \mathbf{p}_n. \tag{24}$$

Defining the scalar product of two vectors as

$$\langle \mathbf{x} | \mathbf{y} \rangle = \mathbf{x}^\dagger \mathbf{R}_p^{-1} \mathbf{y} \tag{25}$$

the objective function becomes simply equal to $||\mathbf{p}_n||^2$. Using this notation, the optimal sound speed estimate can be written as

$$\hat{\mathbf{c}}_{MLM} = \arg\min_{\mathbf{c}} \left[||\mathbf{L}\boldsymbol{\Phi}(\mathbf{c})||^2 - 2\mathrm{Re}\left\{ \langle \mathbf{L}\boldsymbol{\Phi}(\mathbf{c}) | \tilde{\mathbf{p}} \rangle \right\} \right]. \tag{26}$$

By contrast the minimum variance estimate derived in the traditional MFT framework using a linear-system approach can easily be derived using Woodbury's identity as [9]

$$\hat{\mathbf{c}}_{MV} = \arg\min_{\mathbf{c}} \left[||\mathbf{L}\boldsymbol{\Phi}(\mathbf{c})||^2 - \frac{1}{1 + ||\mathbf{L}\boldsymbol{\Phi}(\mathbf{c}_t)||^2} \left| \langle \mathbf{L}\boldsymbol{\Phi}(\mathbf{c}) | \mathbf{L}\boldsymbol{\Phi}(\mathbf{c}_t) \rangle \right|^2 \right] \tag{27}$$

where $\mathbf{c}_t$ represents the true sound speed field. The first term in (27) is usually interpreted in the beamforming literature as the conventional beamforming output [10]. The second term corresponds to the noise nulling operation. Thus, at high SNRs, i.e.,

for large $||\mathbf{L}\Phi(\mathbf{c}_t)||$, the nulling term in (27) cancels out the conventional term and the objective function is minimized for $\hat{\mathbf{c}}_{MV}$ equal to $\mathbf{c}_t$. It is worth noticing that the maximum-likelihood estimator [see (26)] exhibits the same structure, namely a conventional term identical to that in (27) and a nulling term. Although the nulling terms are different, both involve what amounts to a correlation between the data $\tilde{\mathbf{p}}$ or $\mathbf{L}\Phi(\mathbf{c}_t)$ and a replica $\mathbf{L}\Phi(\mathbf{c})$.

III. SPE Inversion

A. Standard Parabolic Equation Model

For the purpose of this paper as well as for computational reasons, we will restrict ourselves to solving the simplified inversion case (Section II-B). Before the set of equations (15) and (16) can be explicitly solved, an acoustic model $\mathcal{B}$ must be specified. We will use the standard parabolic equation model (SPE) for its relevance to a number of operational situations as well as its numerical tractability. The SPE model can be written as [11]

$$\mathcal{B}(\mathbf{p}, \boldsymbol{\eta}) = \mathbf{B}(\boldsymbol{\eta})\mathbf{p} - \mathbf{b}_0 = \mathbf{0} \tag{28}$$

where $\mathbf{b}_0$ is initialized using a Gaussian starter field. The sound speed vector $\mathbf{c}$ has been replaced by the squared index of refraction $\boldsymbol{\eta}$ whose exact mapping is given below [see (34)]. The matrix $\mathbf{B}$ is defined on a computational grid of M nodes in depth by N nodes in range as follows:

$$\mathbf{B}(\boldsymbol{\eta}) = \begin{bmatrix} \mathbf{C}_1^1 & \mathbf{O} & \cdots & \cdots \\ -\mathbf{C}_2^1 & \mathbf{C}_1^2 & \mathbf{O} & \cdots \\ \cdots & \cdots & \cdots & \cdots \\ \mathbf{O} & \cdots & -\mathbf{C}_2^{N-1} & \mathbf{C}_1^N \end{bmatrix}. \tag{29}$$

The matrix $\mathbf{C}_1^m$ is defined at the mth range bin as

$$[\mathbf{C}_1^m]_{jj} = \frac{2ik_0}{\Delta r} - \frac{1}{\Delta z^2} + \frac{1}{2}\eta_{j+(m-1)M}, \quad (j, m) \in [1, M] \times [1, N] \tag{30}$$

$$[\mathbf{C}_1^m]_{j,\, j\pm 1} = \frac{1}{2\Delta z^2}, \quad (j, m) \in [1, M-1] \times [1, N] \tag{31}$$

$$[\mathbf{C}_1^m]_{jl} = 0, \qquad \text{otherwise.} \tag{32}$$

The matrix $\mathbf{C}_2^m$ is defined as

$$\mathbf{C}_2^m = -(\mathbf{C}_1^m)^* \tag{33}$$

where the star denotes complex conjugation. The components $\eta_{j+(m-1)M}$ of the model vector $\boldsymbol{\eta}$ are a monotonic function of the sound speed field

$$\eta_{j+(m-1)M} = k_0^2\left(\frac{c_0^2}{c_{jm}^2} - 1\right) \tag{34}$$

where c_{jm} is the sound speed at the jth depth bin and mth range bin of the computational grid.

B. Inverse Equations

Armed with the explicit dynamical model outlined in the previous section, the derivatives of $\boldsymbol{\mathcal{B}}$ with respect to $\mathbf{p}$ and $\boldsymbol{\eta}$ can be derived. The operator $\boldsymbol{\mathcal{B}}$ is recast in a form more suitable to analytical differentiation

$$\boldsymbol{\mathcal{B}}(\mathbf{p}, \boldsymbol{\eta}) = \mathbf{B}_0\mathbf{p} + \frac{1}{2}(\mathbf{I} + \mathbf{J})\mathcal{D}(\mathbf{p})\boldsymbol{\eta} - \mathbf{b}_0 \tag{35}$$

where $\mathbf{I}$ is the identity matrix and $\mathbf{J}$ has its subdiagonal [corresponding to the η_j^s of $\mathbf{C}_2$ in $\mathbf{B}(\boldsymbol{\eta})$] set to 1. The operator $\mathcal{D}$ maps a vector onto a diagonal matrix whose diagonal elements are given by the former. Thus, the derivatives of $\boldsymbol{\mathcal{B}}$ are

$$\frac{\partial \boldsymbol{\mathcal{B}}(\mathbf{p}, \boldsymbol{\eta})}{\partial \mathbf{p}} = \mathbf{B}(\boldsymbol{\eta}) \tag{36}$$

$$\frac{\partial \boldsymbol{\mathcal{B}}(\mathbf{p}, \boldsymbol{\eta})}{\partial \boldsymbol{\eta}} = \frac{1}{2}(\mathbf{I} + \mathbf{J})\mathcal{D}(\mathbf{p}). \tag{37}$$

We can assume without loss of generality that $\boldsymbol{\eta}$ is zero mean. The system of equations (15) and (16) then becomes

$$\mathbf{L}^\dagger\mathbf{R}_p^{-1}\mathbf{L}\mathbf{p} + \mathbf{B}(\boldsymbol{\eta})^\dagger\mathbf{Q}_b^{-1}(\mathbf{B}(\boldsymbol{\eta})\mathbf{p} - \mathbf{b}_0) = \mathbf{L}^\dagger\mathbf{R}_p^{-1}\tilde{\mathbf{p}} \tag{38}$$

$$\tfrac{1}{2}((\mathbf{I} + \mathbf{J})\mathcal{D}(\mathbf{p}))^\dagger\mathbf{Q}_b^{-1}(\mathbf{B}(\boldsymbol{\eta})\mathbf{p} - \mathbf{b}_0) + \mathbf{S}^{-1}\boldsymbol{\eta} = \mathbf{0}. \tag{39}$$

In the absence of a reliable acoustic model, the inverse covariance $\mathbf{Q}_b^{-1}$ tends to zero, and the system of equations (38) and (39) becomes uncoupled. If the acoustic model is infinitely reliable, i.e., the covariance $\mathbf{Q}_b$ tends to zero, the solution to (38) and (39) becomes independent of the data and is equal to the pressure and sound speed field implicitly assumed in $\boldsymbol{\mathcal{B}}$ within the resolution of the inversion.

C. Inverse Estimates

The system of equations (38) and (39) can be rewritten as

$$\mathbf{p} = \left[\mathbf{L}^\dagger\mathbf{R}_p^{-1}\mathbf{L} + \mathbf{B}(\boldsymbol{\eta})^\dagger\mathbf{Q}_b^{-1}\mathbf{B}(\boldsymbol{\eta})\right]^{-1} \times \left[\mathbf{L}^\dagger\mathbf{R}_p^{-1}\tilde{\mathbf{p}} + \mathbf{B}(\boldsymbol{\eta})^\dagger\mathbf{Q}_b^{-1}\mathbf{b}_0\right] \tag{40}$$

$$\boldsymbol{\eta} = \left[\mathbf{F}(\mathbf{p})^\dagger\mathbf{Q}_b^{-1}\mathbf{F}(\mathbf{p}) + \mathbf{S}^{-1}\right]^{-1}\mathbf{F}(\mathbf{p})^\dagger\mathbf{Q}_b^{-1}(\mathbf{b}_0 - \mathbf{B}_0\mathbf{p}) \tag{41}$$

$$\mathbf{F}(\mathbf{p}) = \tfrac{1}{2}(\mathbf{I} + \mathbf{J})\mathcal{D}(\mathbf{p}) \tag{42}$$

which may be cast in the following symbolic form:

$$\mathbf{p} = \mathbf{f}(\boldsymbol{\eta}) \tag{43}$$

$$\boldsymbol{\eta} = \mathbf{g}(\mathbf{p}). \tag{44}$$

As alluded to in Section II-B, this system might be best solved by iteration. This would however require an error model for $\mathbf{Q}_b$ which is beyond the scope of this paper. Instead, to demonstrate the feasibility of the inversion, we will use the concept of ambiguity surface drawn from the matched-field processing (MFP) literature [12], [11]. Consider the following cost function ϵ:

$$\epsilon(\boldsymbol{\eta}) = \frac{||\mathbf{g}[\mathbf{f}(\boldsymbol{\eta})] - \mathbf{T}\boldsymbol{\eta}||}{||\boldsymbol{\eta}||} \tag{45}$$

where $\mathbf{T}$ is the model resolution of the inverse, i.e., the optimal estimate $\hat{\boldsymbol{\eta}}$ is equal to $\mathbf{T}\boldsymbol{\eta}$. The model resolution captures the fact that even with perfect *a priori* knowledge the true sound speed field can only be recovered within the inherent physical limitations of the observing system. The cost function ϵ will

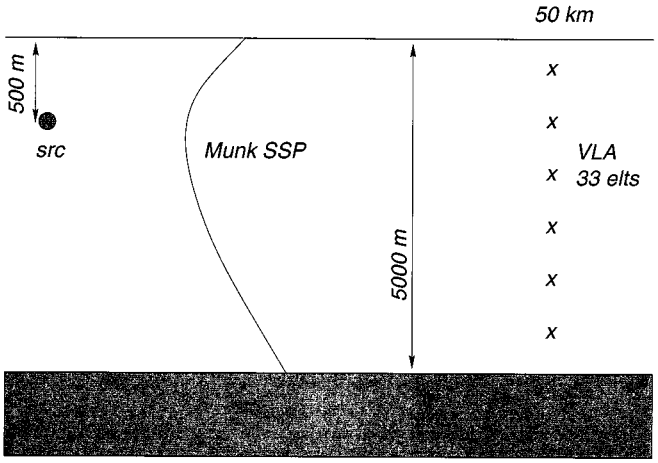

Fig. 1. Deep ocean Munk waveguide. Source frequency: 5 Hz. Ambient noise level: 70 dB re 1 μPa. Source level: 190 dB re 1 μPa 1 m.

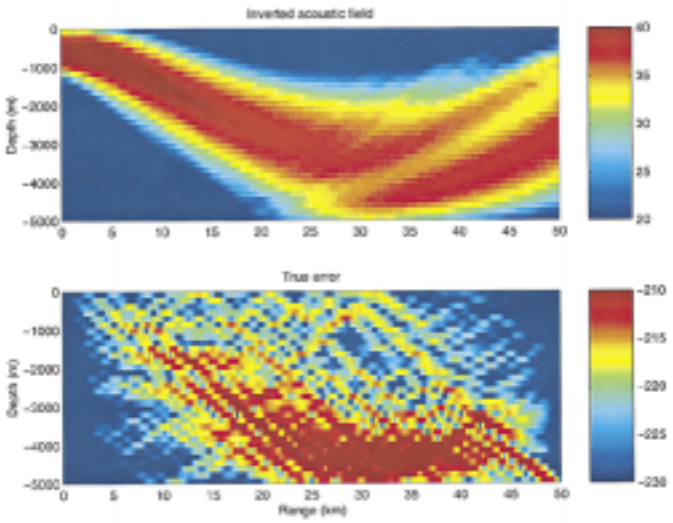

Fig. 2. Top: inverted acoustic pressure field when the true sound speed field is known (dB re 1 μPa). Bottom: true acoustic field error (dB re 1 μPa).

therefore vanish when $\boldsymbol{\eta}$ is equal to the true sound speed field. The cost function might reach a relatively small value for other sound speed fields, thus generating "spurious side lobes" to use MFP terminology. An ambiguity surface can therefore be built by computing ϵ for different values of $\boldsymbol{\eta}$. Alternatively, standard multivariate minimization algorithms may be applied to ϵ. The sound speed field estimate will be computed by identifying the absolute minimum of ϵ.

IV. Numerical Results

A. Framework Validation

The size of the vectors used in (38) and (39) tends to be fairly large and memory-intensive: the size of the pressure field for instance is of order N^2 since it describes a two-dimensional field. The size of matrices such as $\mathbf{B}$ is then of order N^4, where N is the number of grid points in one direction and is typically of the order of 100 and above. The numerical implementation of (40) and (41) is therefore nontrivial and would have been altogether impossible a few years ago due to computational limitations. The purpose of this section is to show that such an implementation is possible today and that sound speed fields can be reasonably estimated using the acoustic data assimilation formulation.

The experimental scenario considered in this paper is shown in Fig. 1. The receiver array consists of 33 elements equally spaced spanning the entire water column at a range of 50 km. The source frequency was set to a low value, 5 Hz, in order to decrease the computational load since this paper is concerned solely with demonstrating the feasibility of the acoustic data assimilation scheme. The receiver noise covariance matrix $\mathbf{R}_p$ is assumed to be of the form $\sigma_p^2\mathbf{I}$, where the ambient noise level σ_p^2 is set equal to 70 dB re 1 μPa. The sound speed profile is a range-independent Munk profile with a channel axis depth of 1300 m (see Fig. 1). The sound speed covariance matrix $\mathbf{S}$ is assumed to be of the form $\sigma_s^2\mathbf{I}$. This covariance matrix really applies to $\boldsymbol{\eta}$, not to the actual sound speed field; the term σ_s^2 was set equal to $2k_0^2$ after calibration of the inversion procedure. Equations (38) and (39) were implemented under the form (43) and (44) using the sparse matrix algebra package UMFPACK [13].

In order to validate the implementation of each equation separately, a pressure field was computed using (43) given the true sound speed field. The result is shown in Fig. 2. The reader should bear in mind that this is not an inversion *per se*, but merely the validation of the numerical implementation of $\mathbf{f}(\boldsymbol{\eta})$ in (43). As expected, the field is recovered with a very good accuracy. In order to be consistent with the parabolic equation model presented above, the Hankel function range dependence of the field is not included. The structure of the acoustic model error covariance $\mathbf{Q}_b$ was assumed to be of the form $\sigma_b^2\mathbf{I}$ where σ_b^2 was set equal to 70 dB re 1 μPa. Conversely, a sound speed field was computed using (44) assuming the true pressure field was known, and the result is shown in Fig. 3 for different values of σ_b^2. Here again the reader should note that this is not an inversion *per se*, but the validation of the numerical implementation of $\mathbf{g}(\boldsymbol{\eta})$ in (44). Note that for the smallest value of σ_b^2 the sound speed field is recovered almost perfectly, except for the region beneath the source, which is not insonified at all and belongs to the null space of the inversion. As the value of σ_b^2 increases, regions that are weakly insonified become impossible to recover.

B. Inversion Results

Having validated our numerical implementation in the previous section, we can now present a simple inversion scenario in which the true sound speed field is initially unknown and is estimated using the measured acoustic data $\tilde{\mathbf{p}}$. This scenario assumes an inclusion of warm water is present at a depth of 1000 m. This inclusion is modeled by the empirical orthogonal function (EOF1) shown in Fig. 4. Sound speed uncertainties associated with surface temperature changes will be subsequently modeled by the exponentially decaying profile (EOF2) also shown in Fig. 4. The resolution matrix $\mathbf{T}$ in (45) is estimated by computing the inverted sound speed field assuming the true sound speed field is the climatological (Munk) profile.

A diagonal pseudoresolution matrix is then constructed by computing each diagonal element such that the true sound speed field is transformed into its inverse estimate. In the absence of

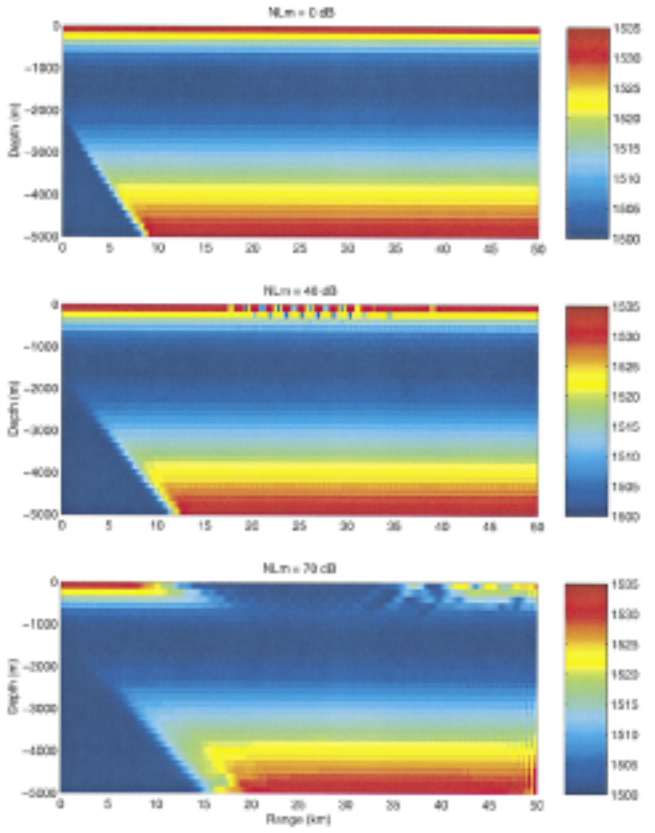

Fig. 3. Inverted sound speed field when the true acoustic field is known. Top: the model noise level is 0 dB. Middle: the model noise level is 40 dB. Bottom: the model noise level is 70 dB.

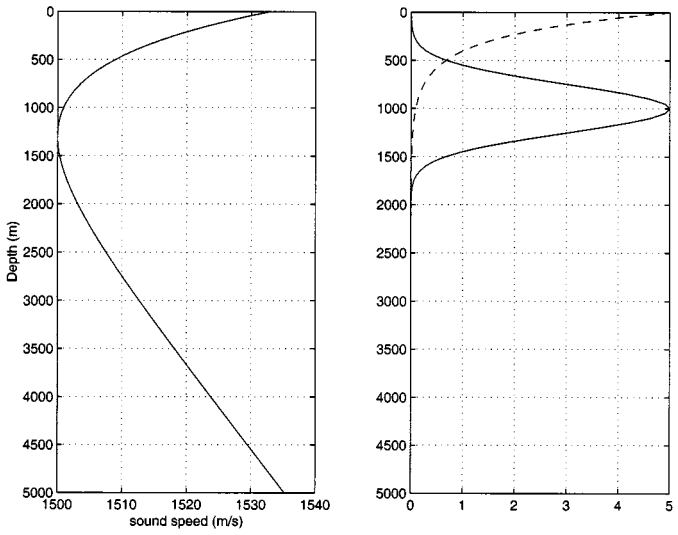

Fig. 4. (a) Climatological (Munk) sound speed profile. (b) Empirical orthogonal functions versus depth (solid line: EOF1; dashed line: EOF2).

a formal resolution estimate, the resolution matrix is approximated by this pseudoresolution matrix when computing $\epsilon(\boldsymbol{\eta})$ as defined in (45).

For the case of no deterministic mismatch, the cost function ϵ is shown in Fig. 5 for different amplitudes of EOF1. As the acoustic model noise σ_b^2 decreases, the main lobe of ϵ becomes

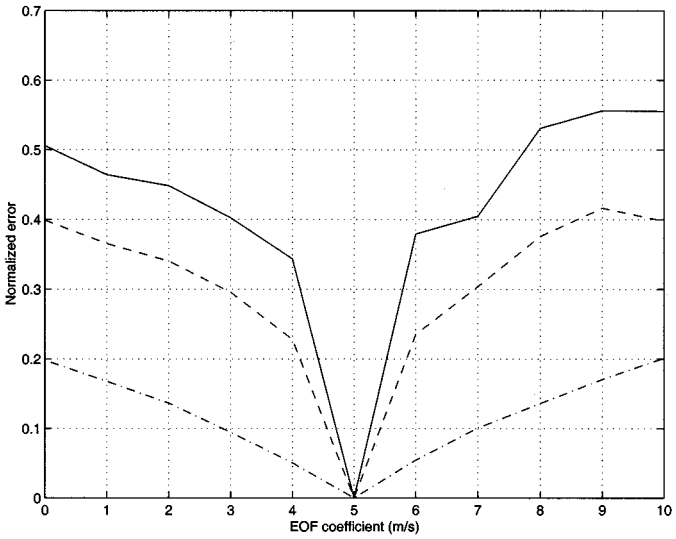

Fig. 5. Cost function $\epsilon(\boldsymbol{\eta})$ versus EOF1 amplitude for different values of σ_b^2 (solid line: $\sigma_b^2 = 0$ dB;, dashed line: $\sigma_b^2 = 20$ dB; dash-dotted line: $\sigma_b^2 = 40$ dB).

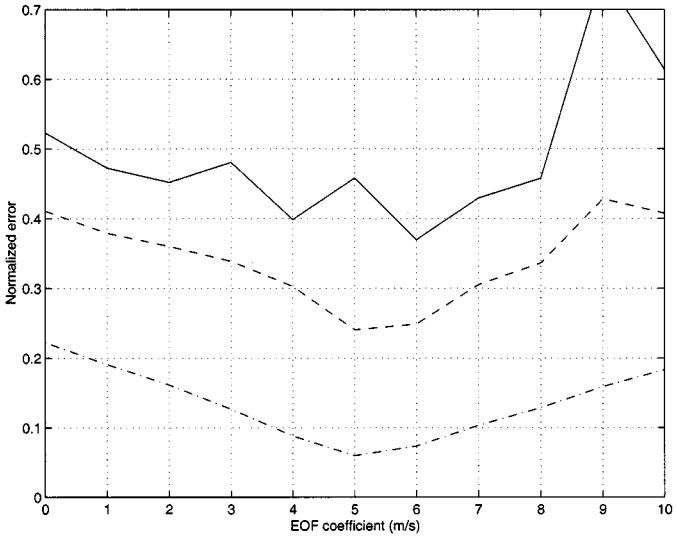

Fig. 6. Cost function $\epsilon(\boldsymbol{\eta})$ versus EOF1 amplitude for different values of σ_b^2 in the presence of environmental mismatch (solid line: $\sigma_b^2 = 0$ dB; dashed line: $\sigma_b^2 = 20$ dB; dash-dotted line: $\sigma_b^2 = 40$ dB).

narrower, indicating that the true magnitude of EOF1 can be identified with a higher accuracy. In other terms, the more accurate the acoustic model, the more accurate the sound speed estimate. The same cost function ϵ is next shown in Fig. 6 in the presence of a 5-m/s sound speed mismatch at the sea surface, modeled by EOF2. The cost function for σ_b^2 equal to 40 dB is almost the same as in the no-mismatch case. The acoustic model is not very accurate, as indicated by the wide main lobe, but it appears to be robust with respect to environmental mismatches. As the model noise decreases, the cost function becomes much more sensitive to environmental mismatch, so that when σ_b^2 is equal to 0 dB, the cost function is no longer well behaved and a clear minimum is no longer identifiable. In other words, the less accurate the acoustic model, the more robust the sound speed estimate but with poorer accuracy. This outlines the inherent trade-off between accuracy and robustness, which

is determined by the choice of σ_b^2, or more generally $\mathbf{Q}_b$. This tradeoff lies at the heart of the inversion methodology presented in this paper: the different sources of noise and error are explicitly accounted for and presumably quantified through the covariances matrices $\mathbf{Q}_a$, $\mathbf{Q}_b$, $\mathbf{R}_p$ and $\mathbf{R}_c$. Mismatches merely increase the level of uncertainty and may be dealt with provided this increase in uncertainty is properly quantified. Possible biases may be straightforwardly added to the formulation without any significant modification. The price paid for this increased uncertainty will be loss of accuracy or resolution. On the other hand, as the inversion is iterated the covariance matrices may be updated and adapted in order to reflect the actual accuracy of the estimate. The inversion can thus be gradually "focused" in a way similar to that suggested by Collins and Kuperman [14].

In addition, it must be noted that by increasing significantly the level of complexity taken into account in the inversion, the present approach increases by an equal amount the computational load required to carry the inversion. Computing (45) currently takes about 6 to 7 min on a Pentium II 450-MHz running Linux, whereas the signal frequency is only 5 Hz. The focus of this paper however is to show the feasibility of such an approach, and as such does not focus on computational performance issues. Although the available computing power is expected to keep increasing at a rapid pace, this added computational load can already be handled through different numerical and analytical means. Firstly, the present analysis inverts the entire acoustic field whereas only the field in the vicinity of the receiver array is needed for sound speed estimation purposes. Restricting the inverted acoustic field in such a way would reduce the size of the estimated acoustic field by 90%, thus yielding a very significant reduction in the size of a number of matrices involved. In order to do so, the field starter $\mathbf{b}_0$ in (28) is first propagated through the water column until the vicinity of the receiver array. Thus, it becomes dependent on the sound speed field, and the associated derivative must be included in the analysis. Secondly, the inversion algorithm requires multiple runs of both the acoustic and the oceanographic (whenever available) models. As such, it lends itself naturally to a parallel and distributed implementation. In some cases however the acoustic field itself needs to be forecast, e.g., for tactical or environmental reasons. In such cases, acoustic data assimilation is at the present time a computational challenge.

V. Summary

The OAT approach to sound speed field estimation has been generalized in this paper to include a variety of sources of information of interest such as an oceanographic model of the sound speed field, direct local sound speed measurements, an arbitrary acoustic propagation model, and full pressure field measurements. This new approach consists of four defining equations:

- a *direct measurement model*, describing the process by which direct, e.g., CTD, measurements are acquired: it relates the directly measured sound speed field to the true sound speed field;
- an *oceanographic model*, imposing a general constraint on the true sound speed field; it may represent the circulation model available for the region of interest;
- an *acoustic propagation model*, relating the true sound speed field to the true acoustic pressure field;
- an *acoustic measurement model*, describing the process by which acoustic measurements are acquired.

A solution to this set of four equations can be computed in a least square sense. The resulting sound speed and pressure field estimates agree with both the data and the models within their respective error bounds. The strengths of this acoustic data assimilation approach are: 1) all dynamical and measurement processes are laid out explicitly and exactly; 2) any acoustic propagation model may be used; 3) all error statistics must be explicitly quantified, in particular model error statistics; and 4) full field acoustic data are used. Environmental or system mismatches are quantified through appropriate error statistics, thus affecting the inversion resolution. By contrast, OAT makes a number of implicit assumptions in its measurement model. More importantly, neither OAT nor MFT explicitly quantifies the inaccuracies of the underlying acoustic model, thus leading to a heightened sensitivity to mismatch since the corresponding inversion algorithms assume all modeling and system information to be exact. On the other hand, by increasing the complexity and the amount of information taken into account in the inversion, the computational load is significantly increased. However, this increase can be mitigated by the use of sparse matrix algebra as well as parallel and distributed computing techniques. These as well as inclusion of oceanographic models are currently being investigated within the framework of an acoustically focused oceanographic sampling (AFOS) network.

Acknowledgment

The authors gratefully acknowledge discussions with Dr. P. Lermusiaux of Harvard University regarding data assimilation concepts and their application to the tomographic problem described in this paper. The authors also thank the reviewers for several useful suggestions.

References

[1] H. Schmidt, J. G. Bellingham, and P. Elisseeff, "Acoustically focused oceanographic sampling in coastal environments," in *Rapid Environmental Assessment*. ser. Conference Proceedings Series CP-44, E. Pouliquen, A. D. Kirwan, and R. T. Pearson, Eds. La Spezia, Italy: SACLANTCEN, 1997, pp. 145–151.

[2] P. Elisseeff, H. Schmidt, M. Johnson, D. Herold, N. R. Chapman, and M. M. McDonald, "Acoustic tomography of a coastal front in Haro Strait, British Columbia," *J. Acoust. Soc. Amer.*, vol. 106, pp. 169–184, 1999.

[3] W. Munk, P. Worcester, and C. Wunsch, *Ocean Acoustic Tomography*. Cambridge, U.K.: Cambridge Univ. Press, 1995.

[4] A. R. Robinson, P. F. J. Lermusiaux, and N. Q. Sloan, "Data assimilation," in *The Sea*, K. H. Brink and A. R. Robinson, Eds. New York: Wiley, 1998, vol. 10, pp. 541–594.

[5] E. K. Skarsoulis, "A matched-peak inversion approach for ocean acoustic travel-time tomography," *J. Acoust. Soc. Amer.*, vol. 107, pp. 1324–1332, 2000.

[6] R. Giering and T. Kaminski, "Recipes for adjoint code construction," *ACM Trans. Math. Software*, vol. 24, pp. 437–474, 1998.

[7] A. Tolstoy, *Matched-Field Processing for Underwater Acoustics*. Singapore: World Scientific, 1993.

[8] A. B. Baggeroer and H. Schmidt, "Cramer–Rao bounds for matched field tomography and ocean acoustic tomography," in *Proc. ICASSP*, 1995, pp. 2763–2766.

[9] A. P. Sage and J. L. Melsa, *Estimation Theory With Applications to Communications and Control*. New York: McGraw-Hill, 1971.

[10] D. H. Johnson and D. E. Dudgeon, *Array Signal Processing—Concepts and Techniques*. Englewood Cliffs, NJ: Prentice-Hall, 1993.
[11] F. B. Jensen, W. A. Kuperman, M. B. Porter, and H. Schmidt, *Computational Ocean Acoustics*. College Park, MD: Amer. Inst. Physics, 1994.
[12] A. B. Baggeroer, W. A. Kuperman, and H. Schmidt, "Matched field processing: Source localization in correlated noise as an optimum parameter estimation problem," *J. Acoust. Soc. Amer.*, vol. 83, pp. 571–587, 1988.
[13] T. A. Davis and I. A. Duff, "An unsymmetric-pattern multifrontal method for sparse LU factorization," *SIAM J. Matrix Anal. Applicat.*, vol. 18, pp. 140–158, 1997.
[14] M. D. Collins and W. A. Kuperman, "Focalization: Environmental focusing and source localization," *J. Acoust. Soc. Amer.*, vol. 90, pp. 1410–1422, 1991.

Pierre Elisseeff graduated from Ecole Centrale Paris (France) in 1991. He received the M.S. degree in ocean engineering from Florida Atlantic University, Boca Raton, in 1991 and the Ph.D. degree in ocean engineering from the Massachusetts Institute of Technology (MIT), Cambridge, in 1998.

From 1998 to 1999, he was a Post-Doctoral Associate in the Ocean Acoustics Group, MIT, and a member of the Scientific Council of the Littoral Ocean Observation and Prediction System (LOOPS) project. He is currently an associate with Dean & Company, a strategy consulting firm based in Vienna, VA, and focuses on mergers and acquisitions in the telecommunications industry. He is a Level II candidate in the CFA program of the American Institute of Management Research.

Henrik Schmidt received the M.S. degree in civil engineering and the Ph.D. degree in experimental mechanics from the Technical University of Denmark in 1974 and 1978, respectively.

Holding positions of Research Fellow from 1978 to 1980 at the Technical University of Denmark, and from 1980 to 1982 at Risoe National Laboratory, Denmark, he worked on numerical modeling of wave propagation and scattering phenomena in relation to nondestructive testing of structures. From 1982 to 1987, he was Scientist and Senior Scientist at SACLANT Undersea Research Center, La Spezia, Italy, where he developed the SAFARI code for modeling seismo-acoustic propagation in ocean waveguides. In 1987, he joined the Massachusetts Institute of Technology, Cambridge, where he is currently Professor and Associate Head of Ocean Engineering. His primary research interest is the interaction of underwater sound with seismic waves in the seabed and the Arctic ice cover. Other interests include computational acoustics and matched-field processing, and the use of acoustics in autonomous oceanographic sampling networks.

Dr. Schmidt is a Fellow of the Acoustical Society of America and a member of the Society of Exploration Geophysicists.

Wen Xu (S'96–A'01–M'02) received the B.E. degree in electrical engineering from the University of Science and Technology of China, Hefei, China, in 1990, the M.S. degree in acoustics from the Institute of Acoustics, Chinese Academy of Sciences, Beijing, China, in 1993, and the M.S. and Ph.D. degrees in oceanographic engineering from the Massachusetts Institute of Technology (MIT), Cambridge, in 1998 and 2001, respectively.

From 1993 to 1996, he was a Research Engineer at the Institute of Acoustics, Chinese Academy of Sciences. He is presently a Research Scientist with the Ocean Acoustics Group, MIT. His research interests include signal processing algorithms and systems and underwater acoustics.

Dr. Xu is a member of the Acoustical Society of America and Sigma Xi.